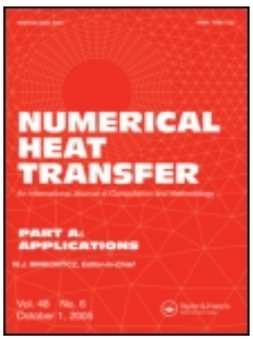

Numerical Heat Transfer, Part A: Applications

ISSN: 1040-7782 (Print) 1521-0634 (Online) Journal homepage: http://www.tandfonline.com/loi/unht20

LAMINAR NATURAL CONVECTION HEAT TRANSFER IN AN ECCENTRIC RHOMBIC ANNULUS

F. Moukalled & S. Acharya

To cite this article: F. Moukalled & S. Acharya (1994) LAMINAR NATURAL CONVECTION HEAT TRANSFER IN AN ECCENTRIC RHOMBIC ANNULUS, Numerical Heat Transfer, Part A: Applications, 26:5, 551-568, DOI: 10.1080/10407789408956009

To link to this article: http://dx.doi.org/10.1080/10407789408956009

LAMINAR NATURAL CONVECTION HEAT TRANSFER IN AN ECCENTRIC RHOMBIC ANNULUS

F. Moukalled
Faculty of Engineering and Architecture, American University of Beirut, Beirut, Lebanon

S. Acharya
Mechanical Engineering Department, Louisiana State University, 2513B CEBA, Baton Rouge, Louisiana 70803 USA

The effect of vertical eccentricity on natural convection in a rhombic annulus is studied numerically for enclosure gap values (E_g) ***of 0.5 and 0.75, eccentricity*** (ε) ***values from*** -0.25 ***to 0.25, and Rayleigh numbers (Ra) from*** 10^4 ***to*** 10^8***. Negative values of*** ε ***(inner rhombus displaced downward) lead to an increase in heat transfer. At low Ra there is a critical positive*** ε ***for which the flow strength is a maximum. At high Ra, increasing positive*** ε ***results in a decrease in the flow strength and heat transfer. For any*** $\varepsilon > 0$ ***there is a critical Ra, beyond which there is a decrease in the total heat transfer. This critical Ra increases with decreasing*** E_g ***values.***

INTRODUCTION

Natural convection heat transfer in rectangular enclosures and cylindrical annuli has been extensively studied, and a recent review on this topic is given by Ostrach [1]. However, natural convection heat transfer in enclosures with a more complex geometry has received rather limited attention.

Several experimental, numerical, and analytical studies on natural convection in cylindrical annuli have been reported. Kuehn and Goldstein [2, 3] have reported a thorough literature survey and have also performed a detailed study of convection within a horizontal annulus. Custer and Shaughnessy [4] obtained analytical solutions for laminar flow of very low Prandtl number fluids in a horizontal annulus. Turbulent flow computations were subsequently reported by Farouk and Guceri [5]. More recent studies on natural convection in cylindrical annuli include those of Castrejon and Spalding [6], Kumar [7], and Kolesnikov and Bubnovich [8].

Received 25 May 1993; accepted 28 January 1994.

The financial support provided by the University Research Board of the American University of Beirut through grant 18-4217 is gratefully acknowledged.

Address correspondence to S. Acharya, Mechanical Engineering Department, Louisiana State University, 2513B CEBA, Baton Rouge, LA 70803, USA.

Numerical Heat Transfer, Part A, 26:551–568, 1994

1040–7782/94 $10.00 + .00

NOMENCLATURE

c_p	specific heat of fluid	x, X	dimensional and dimensionless horizontal coordinate
E_g	dimensionless enclosure gap $[= (L_o - L_i)/L_o]$	y, Y	dimensional and dimensionless vertical coordinate
g	acceleration due to gravity	β	coefficient of thermal expansion
$h, \bar{h}$	local and average convection heat transfer coefficient	$\varepsilon', \varepsilon$	dimensional and dimensionless eccentricity $(\varepsilon = \varepsilon'/L_o)$
k	thermal conductivity of fluid	θ	dimensionless temperature
L_i, L_o	main diagonal length of the inner and outer rhombic duct	ν	kinematic viscosity
Nu, $\overline{\text{Nu}}$	local and average Nusselt number	ρ	density
p	thermodynamic pressure	ψ	stream function
P	dimensionless pressure	Ω	rhombic angle
Pr	Prandtl number $(= \mu c_p/k)$		
Ra	Rayleigh number $[= g\beta(T_h - T_c)L_0^3/\nu\alpha]$	**Subscripts**	
s	distance along the wall	c	cold wall
S	arc length	h	hot wall
T	dimensional temperature	i	inner pipe
u, U	dimensional and dimensionless velocity in x direction	l	lower part $(0 < s/s_{max} \leq 0.5)$
		max	maximum value
v, V	dimensional and dimensionless velocity in y direction	o	outer pipe
		u	upper part $(0.5 < s/s_{max} < 1)$

Natural convection heat transfer in eccentric horizontal cylindrical annuli has also been studied. Typical studies include those reported in Refs. [9–14]. At very small eccentricities the flow field and heat transfer characteristics were found to be unaffected. Effects were noticed to be significant at large eccentricities.

As noted earlier, studies on natural convection heat transfer in an enclosure between complex geometries are rather limited. Chang et al. [15] performed an experimental and numerical study of natural convection around a square cylinder placed concentrically in a horizontal circular cylinder. Lee and Lee [16] examined the heat transfer characteristics in the annuli between confocal elliptic cylinders. Heat transfer measurements in the enclosure between a cubical outer body and a cylindrical, spherical, or cubical inner body were reported by Warrington and Powe [17]. Boyd [18] reported heat transfer experiments for natural convection in a spent nuclear fuel shipping cask represented by a horizontal annulus with a hexagonal inner body and a circular outer body. Glakpe and Asfaw [19] reported predictions for a similar hexagonal geometry. Moukalled et al. [20] have recently studied laminar natural convection heat transfer in an enclosure between two concentric rhombic bodies.

The present research is intended to investigate natural convection in the annulus between two horizontal eccentric bodies of rhombic cross sections (Figure 1). Possible applications of such a geometry are in thermal storage, and in the transportation and storage of spent nuclear material and assemblies. Results are compared with those reported by Moukalled et al. [20] for the concentric case in order to reveal the effects of eccentricity on the heat transfer and the flow field.

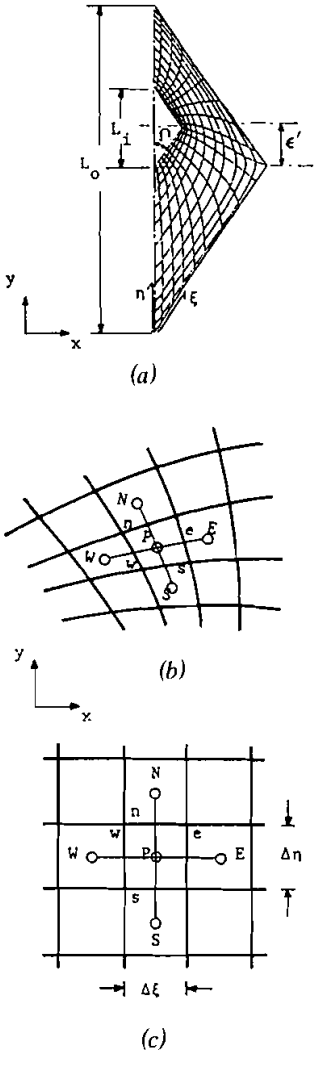

Figure 1. (*a*) Physical domain and an illustrative grid; (*b*) control volume in physical plane; (*c*) control volume in transformed plane.

GOVERNING EQUATIONS

Figure 1 shows a physical schematic of the eccentric rhombic enclosure, which consists of an inner rhombic body that is heated and maintained at a uniform temperature T_h and is eccentrically placed in a cooled outer rhombic body maintained at a uniform temperature T_c. The working fluid is taken to be air, and the flow is considered to be steady, laminar, and two-dimensional. The fluid is assumed to satisfy the Boussinesq approximation, according to which the density appearing in the body force term is related to temperature by the following equation:

$$\rho = \rho_c[1 - \beta(T - T_c)] \tag{1}$$

where ρ_c, T_c, and β are the reference density, the reference temperature, and the coefficient of thermal expansion, respectively. In the present paper, conditions at the cold wall temperature are assumed to be the reference conditions. The dimensionless variables chosen are

$$X = x/L_o \qquad Y = y/L_o \tag{2}$$

$$U = \frac{u}{\nu/L_o} \qquad V = \frac{v}{\nu/L_o} \tag{3}$$

$$P = \frac{p + \rho g y}{\rho(\nu/L_o)^2} \qquad \theta = \frac{T - T_c}{T_h - T_c} \tag{4}$$

With the aforesaid assumptions and dimensionless variables, the governing differential equations in nondimensional form can be written as

$$\nabla \cdot \mathbf{U} = 0 \tag{5}$$

$$\mathbf{U} \cdot \nabla U = -P_X + \nabla^2 U \tag{6}$$

$$\mathbf{U} \cdot \nabla V = -P_Y + \nabla^2 V + \frac{\mathrm{Ra}\,\theta}{\mathrm{Pr}} \tag{7}$$

$$\mathbf{U} \cdot \nabla \theta = \frac{\nabla^2 \theta}{\mathrm{Pr}} \tag{8}$$

Due to the symmetry around the y axis, computations are performed in only the right half of the physical domain. The boundary conditions used are

$$U = V = 0 \tag{9}$$

on all walls,

$$V_x = \theta_x = U = 0 \tag{10}$$

on vertical symmetry lines,

$$\theta = 0 \tag{11}$$

on the outer cold wall, and

$$\theta = 1 \tag{12}$$

on the inner hot wall.

SOLUTION PROCEDURE

Due to the geometry of the eccentric rhombic annulus, a curvilinear coordinate system is used. To obtain the numerical solution to the governing differential

equations, Eqs. (5)–(8) are first transformed into curvilinear coordinates (ξ, η) and then discretized in the ξ, η computational domain using a control-volume-based procedure. The computational domain is generated by solving a system of Poisson equations for $x(\xi, \eta)$ and $y(\xi, \eta)$ as described by Thompson [21]. An illustrative grid network generated is shown in Figure 1. The transformed governing differential equations are discretized by first integrating them over each control volume and then using Green's theorem to replace the volume integral by the surface integral. With suitable profile approximations in each coordinate direction (the power law approximation of Patankar [22] is used in this study), a system of algebraic equations results and can be solved iteratively.

The solution to the resulting algebraic system of equations is generally obtained on a staggered grid to avoid checkerboard pressure and velocity fields. In curvilinear coordinates this becomes cumbersome, since three sets of grid positions (one each for the two components of velocity and one for pressure) and associated metric quantities have to be calculated and stored. It is therefore desirable to use a nonstaggered grid arrangement that will suppress checkerboard pressure and velocity fields. In this paper a nonstaggered grid arrangement is adopted, and the method of Rhie and Chow [23] that embodies the semi-implicit method for pressure linked equations (SIMPLE) algorithm of Patankar [22] is used to suppress oscillatory checkerboard fields. In the SIMPLE method an equation for pressure correction (p') is derived from the continuity equation, and a predictor-corrector procedure is invoked to update pressures and velocities until the velocity field satisfies both momentum and continuity equations.

Results have been generated on a 42×32 nonuniform grid with denser clustering of the grid points near the walls, where higher gradients are expected. The choice of the grid point distribution is based on a number of preliminary calculations with successively finer grids. Comparison of the solution on a 42×32 grid with the solution on a 62×42 grid revealed that the maximum differences were less than 2.15% in the peak Nusselt number value and less than 1.87% in the maximum strength of the flow $(|\psi_{max}|)$. Conservation of mass, momentum, and energy was found to be satisfied to within 0.01% in each control volume.

RESULTS AND DISCUSSION

The governing parameters in the problem are the dimensionless enclosure gap E_g, the rhombic angle Ω, the Rayleigh number Ra, the Prandtl number Pr, and the eccentricity ε. Eccentricity is defined as the dimensionless vertical distance between the centers of the inner and outer cylinders and is taken to be positive for upward displacement of the inner cylinder. In order to reduce the number of parameters involved, Ω is fixed at 30° and Pr is assigned the value of 0.71, corresponding to air. Results are obtained for two different values of E_g (= 0.75 and 0.5), with Ra ranging from 10^4 to 10^8 and ε varying from -0.25 to 0.25. Results generated are presented in the form of streamline, isotherm, and Nu plots. In addition, maximum stream function and average Nu values are tabulated in Tables 1–3.

Table 1. Maximum Absolute Values of the Stream Function

	$E_g = 0.75$					$E_g = 0.5$		
Ra	$\varepsilon = -0.25$	$\varepsilon = -0.125$	$\varepsilon = 0$	$\varepsilon = 0.125$	$\varepsilon = 0.25$	$\varepsilon = -0.125$	$\varepsilon = 0$	$\varepsilon = 0.125$
10^4	0.378	0.377	0.246	0.347	0.317	0.211	0.0754	0.208
10^5	5.02	4.36	2.37	2.55	1.93	2.2	0.753	1.9
10^6	22.8	21.3	14.2	9.84	6.06	15.2	7.12	9.81
10^7	62.8	55.5	39.1	27.5	15.3	46.3	35.7	23.5
5×10^7	96.9	81.2	64.1	50.3	29.8	83.7	64.6	43
10^8	120	99.3	81.2	62.6	38.2	106	79	57

Streamlines and Isotherms

The influence of ε on the flow and temperature fields is revealed by the isotherm and streamline plots depicted in Figures 2–7. Figures 2–4 are for $E_g = 0.75$, while Figures 5–7 are for $E_g = 0.5$. Streamlines are normalized by the maximum stream function values ψ_{max} in the field. The ψ_{max} values are presented in Table 1 and are also indicated alongside the figures. Results for the concentric annulus ($\varepsilon = 0$), reported earlier, are included for comparison.

At low values of Ra the convective flow is weak (see Figures 2 and 5, for example) and is characterized by a single eddy. Isotherms indicate a conductionlike behavior, and flow-induced stratification effects are very small. The flow patterns and isotherms for both positive and negative ε are qualitatively similar. At low Ra, where stratification effects are weak, both positive and negative ε lead to an increase in the convective flow strength, which occurs above the inner rhombus for negative ε and below the inner rhombus for positive ε. The increase in flow strength on one side of the eccentric annulus is linked to the greater flow area or length scale on that side resulting from moving the inner rhombus up or down. At $Ra = 10^4$, a careful examination of the isotherms for $\varepsilon = 0.25$ (Figure 2j) and for $\varepsilon = -0.25$ (Figure 2f) indicates a stratification (stabilizing) in the lower half of Figure 2j compared with the destabilizing isotherm pattern in the upper half of Figure 2f. Therefore, the flow strength for negative ε is higher than the flow strength for positive ε.

Table 2. Average Nusselt Number Values

	$E_g = 0.75$					$E_g = 0.5$		
Ra	$\varepsilon = -0.25$	$\varepsilon = -0.125$	$\varepsilon = 0$	$\varepsilon = 0.125$	$\varepsilon = 0.25$	$\varepsilon = -0.125$	$\varepsilon = 0$	$\varepsilon = 0.125$
Conduction	4.15	2.50	2.23	2.50	4.15	6.62	5.08	6.62
10^4	4.33	2.57	2.23	2.55	4.16	6.72	5.08	7.29
10^5	4.65	2.97	2.37	2.70	4.27	6.87	5.08	7.33
10^6	5.89	4.76	4.49	4.12	4.90	8.93	5.94	8.06
10^7	8.57	8.74	8.10	7.86	7.15	12.77	11.55	10.74
5×10^7	13.91	13.49	12.70	12.07	11.43	18.9	18.29	16.37
10^8	17.24	16.51	15.51	14.75	13.92	23.28	22.21	19.99

Table 3. Average Nusselt Number Values over the Lower and Upper Half of the Cold Wall ($E_g = 0.75$)

	Lower half					Upper half				
Ra	$\varepsilon = -0.25$	$\varepsilon = -0.125$	$\varepsilon = 0$	$\varepsilon = 0.125$	$\varepsilon = 0.25$	$\varepsilon = -0.25$	$\varepsilon = -0.125$	$\varepsilon = 0$	$\varepsilon = 0.125$	$\varepsilon = 0.25$
10^4	7.92	3.88	2.19	1.13	0.46	0.74	1.26	2.27	3.97	7.86
10^5	7.31	3.21	1.65	0.83	0.28	1.99	2.73	3.10	4.57	8.26
10^6	6.81	2.39	1.11	0.69	0.19	4.97	7.13	7.88	7.55	9.61
10^7	5.97	3.22	2.07	0.84	0.12	11.17	14.26	14.13	14.88	14.18
5×10^7	6.75	4.65	3.05	1.07	0.096	21.07	22.33	22.35	23.07	22.76
10^8	7.84	5.67	3.33	1.23	0.081	26.64	27.35	27.69	28.27	27.76

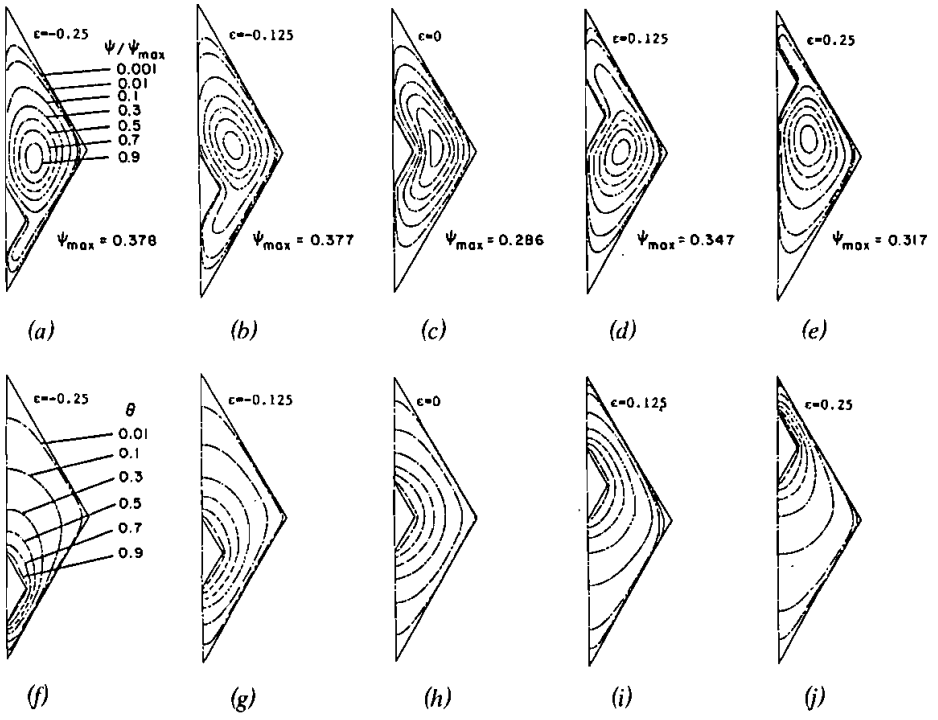

Figure 2. Streamline and isotherm plots ($E_g = 0.75$, Ra $= 10^4$).

As Ra is increased from 10^4 (Figure 2) to 10^8 (Figure 4), the convective flow strength for all cases ($\varepsilon \geq 0$, $\varepsilon < 0$) expectedly increases. However, flow-induced thermal stratification effects become increasingly important at higher Ra, and in view of the fact that the cooled outer surface is proportionately larger than the heated inner surface, stratification effects are primarily significant below the horizontal diagonal of the inner rhombus. Therefore for positive ε, where a greater proportion of the flow area is in the bottom half, stratification effects are significantly more important than in the case with negative ε. Thus, at higher Ra, where stratification is important, the velocity and temperature profiles for $\varepsilon > 0$ are quite different from the corresponding profiles for $\varepsilon < 0$. As the inner rhombus is moved upward ($\varepsilon > 0$), flow-induced thermal stratification below the inner rhombus increases, leading to a reduction in the flow strength. This is clearly seen from the ψ_{max} values listed in Figures 3 and 4, and in Table 1. The thermally stratified field for $\varepsilon > 0$ is clearly evident in the isotherm patterns, for example, Figure 4j.

For negative ε, flow-induced thermal stratification in the primary flow area above the inner rhombus does not occur, and the effect of moving the inner rhombus downward is to increase the primary flow area or the effective length scale and, thus, to increase the convective flow strength above the inner rhombus. At the higher Ra (Figure 4) the isotherm and flow patterns clearly reveal the boundary layer behavior along the upper half of the cooled wall and lower half of the heated wall. In view of the stronger convective flow strength at negative ε, the

boundary layer behavior is much stronger for $\varepsilon < 0$ (compare Figure 4f for $\varepsilon = -0.25$ with Figure 4j for $\varepsilon = 0.25$).

As noted above, and as shown in Table 1, for low Ra, the ψ_{max} for $\varepsilon > 0$ is greater than the ψ_{max} for $\varepsilon = 0$ (see Figure 2), while at higher Ra, the ψ_{max} for $\varepsilon > 0$ is less than the ψ_{max} for $\varepsilon = 0$ (see Figure 3). Thus, for positive ε, there exists a value of Ra for which the maximum strength of the flow is unaffected by ε within a certain bound for ε. This critical value for Ra decreases with ε and increases with E_g (see Table 1). In addition, at a constant Ra, Table 1 indicates the presence of an optimum positive ε that maximizes the strength of the flow. The value of this ε decreases with increasing Ra. To explain this behavior, it is noted that as ε is increased from 0, two counteracting effects occur. The first is that the primary flow area below the horizontal diagonal increases, leading to an increase in the flow strength. The second effect is that flow-induced thermal stratification in the lower half increases, and this leads to a reduction in the flow strength. With increasing Ra, the second effect becomes more important and therefore the value of ε for which ψ_{max} peaks is smaller at a larger value of Ra.

At low and moderate Ra (Figures 2, 3, 5, and 6) the flow field is characterized by an eddy rotating in the clockwise direction. At high Ra (Figures 4 and 7) the recirculating flow exhibits two vortex cores within one large eddy rotating clockwise. In addition, at high Ra, flow separation occurs in the lower part of the domain, leading to a counterclockwise separated eddy. Flow separation is caused by thermal stratification in the lower part of the rhombic annulus, due to which the

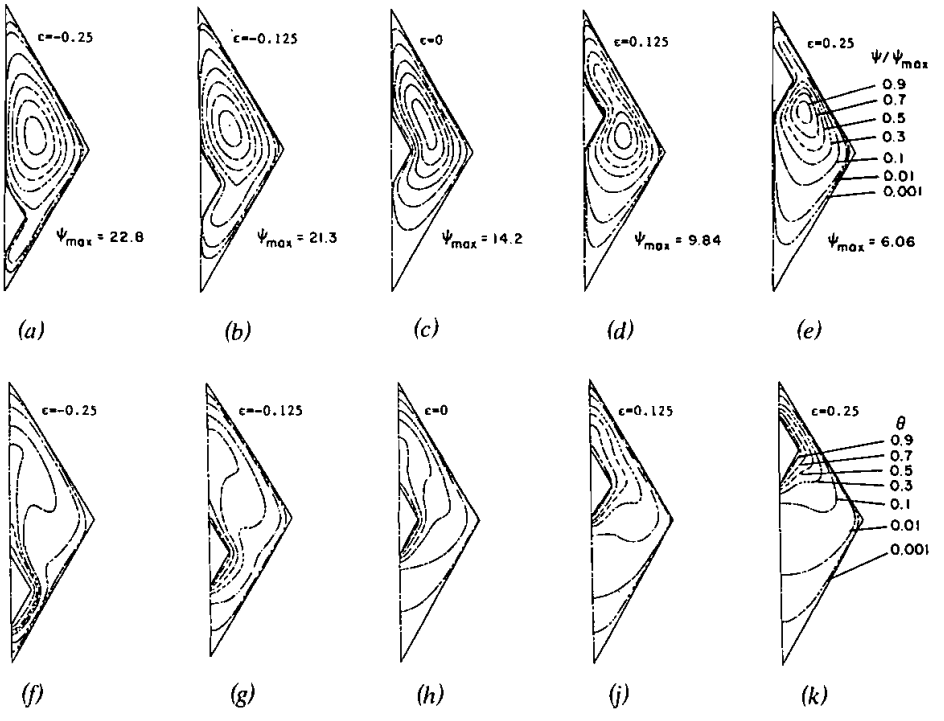

Figure 3. Streamline and isotherm plots ($E_g = 0.75$, Ra = 10^6).

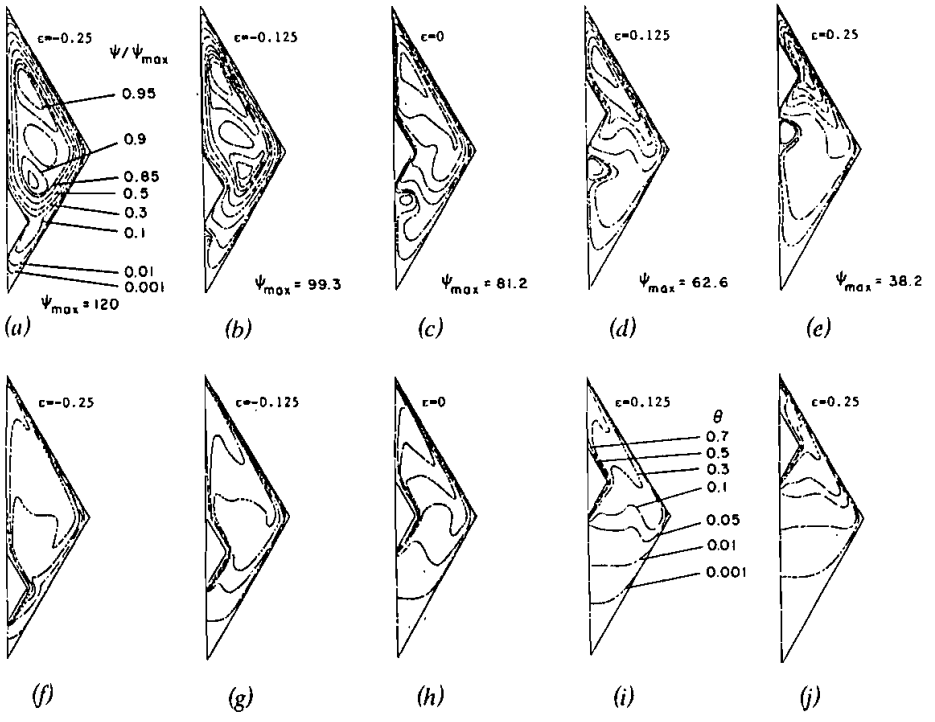

Figure 4. Streamline and isotherm plots ($E_g = 0.75$, Ra $= 10^8$).

flow descending the cooled wall cannot easily penetrate the lower region. As seen in Figures 4 and 7, the flow is essentially stagnant or very weak in the thermally stratified region, and thus as the air adjacent to the heated inner rhombus rises, it entrains a smaller fraction of air upward from the stratified region, and instead, more of the air is entrained sideways above the stratified region. This leads to a separated anticlockwise eddy. The size of this eddy is seen to decrease with increasing eccentricity for $\varepsilon > 0$ and to increase with increasing eccentricity for $\varepsilon > 0$. For $\varepsilon < 0$ the convective area below the inner rhombus is reduced, causing a less significant temperature stratification in the lower part. Thus, the penetration of this area by the flow is easier. In fact, for $\varepsilon = -0.25$, separation does not occur. In contrast, for $\varepsilon > 0$, a larger stratified stagnant area is seen in the lower part of the enclosure, inhibiting the motion of the fluid and causing a larger separation eddy.

The effect of decreasing the dimensionless gap ratio from $E_g = 0.75$ (Figures 2–4) to $E_g = 0.5$ (Figures 5–7) is to decrease the primary flow area and thus the convective flow strength. Lower velocities imply smaller flow-induced stratification effects below the inner rhombus, and therefore, as seen from Table 1, for positive ε, the critical Ra at which ψ_{max} decreases with ε is larger at $E_g = 0.5$ compared with the corresponding value at $E_g = 0.75$. Figure 7c when compared with Figure 4d shows further that the counterrotating separated eddy is smaller and weaker for the smaller E_g value due to the lower associated thermal stratification effect.

While some of the flow field features in the rhombic annulus are similar to that in the cylindrical annulus, there are a number of important notable differences. These include not only the differences in the strength of the flow patterns and the extent of the stratification effects, but also differences in the basic flow and isotherm pattern itself. For example, at higher Ra (of the order of 10^5 and higher), Projahn et al. [9] reported the formation of a counterrotating eddy above the inner cylinder in eccentric cylindrical annulus with $\varepsilon \approx 0.2$ and E_g of the order of 0.625. The formation of this counterrotating eddy distorts the Nusselt number profiles and shifts the peak along the outer wall from near $\theta = 0$ to about $\theta = 30°-40°$ (θ refers to the angular position measured from the upper vertical centerline). For the configuration considered in this paper, for comparable values of ε, E_g, and Ra, no separate eddy above the inner cylinder is noted; on the contrary, at sufficiently high Ra a counterrotating eddy is noted in the stratified region below the inner rhombus.

Nusselt Numbers

Attention will now be focused on the effect of ε on the total heat transfer. This will be done by presenting the average Nu for all cases under consideration (Table 2) and by plotting the local Nu distribution along the hot inner and cold

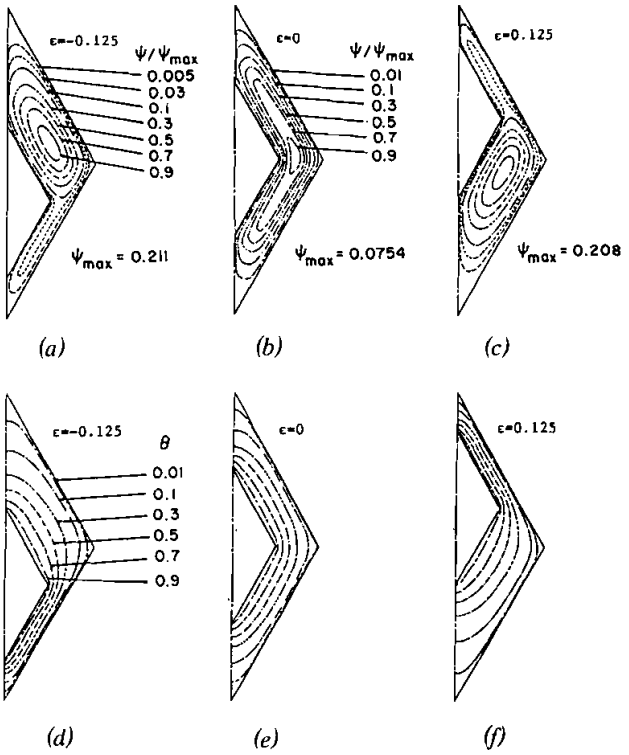

Figure 5. Streamline and isotherm plots ($E_g = 0.5$, Ra = 10^4).

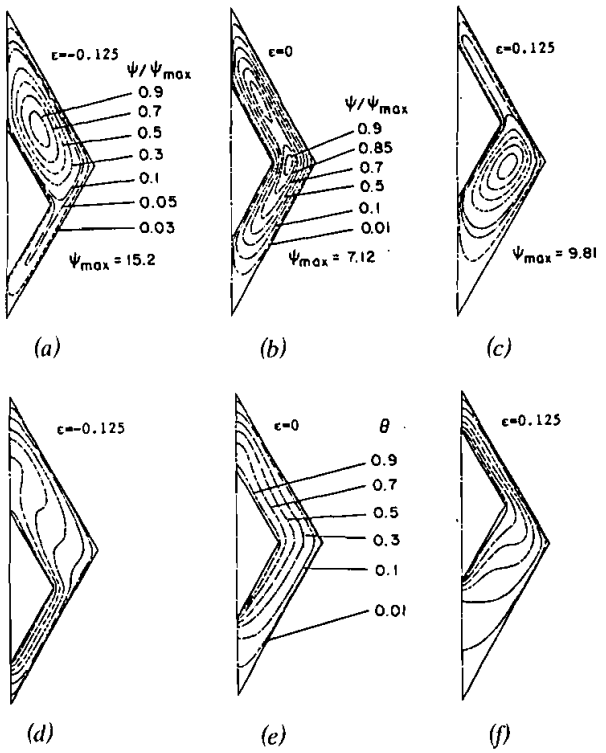

Figure 6. Streamline and isotherm plots ($E_g = 0.5$, Ra = 10^6).

outer walls for some selected cases (Figures 8–10). The local and average Nu at the inner and outer walls were computed using the following definitions:

$$\mathrm{Nu}_i = -\frac{\partial T/\partial n|_i}{(T_i - T_o)/L_i} \qquad \mathrm{Nu}_o = -\frac{\partial T/\partial n|_o}{(T_i - T_o)/L_o} \tag{13}$$

$$\overline{\mathrm{Nu}_i} = \int_0^{s_{\max}} \mathrm{Nu}_i \, ds/s_{\max} \qquad \overline{\mathrm{Nu}_o} = \int_0^{s_{\max}} \mathrm{Nu}_o \, ds/s_{\max} \tag{14}$$

where n denotes the normal distance from the wall, s is distance along the wall measured from its lowest point, and $s_{\max}$ is the maximum possible length. Since $\overline{\mathrm{Nu}_i} = \overline{\mathrm{Nu}_o}$, the subscript will be dropped and the average heat transfer will be denoted by $\overline{\mathrm{Nu}}$.

The Nu as defined above represents the heat flux ($-k\,\partial T/\partial n$) made dimensionless with $(T_i - T_o)/(L/k)$. Nu for pure conduction can also be defined and represents the ratio of the two-dimensional conduction heat flux made dimensionless with the corresponding one-dimensional conduction value.

Figures 8–11 show the Nu distributions along the hot and cold walls. Values are plotted as a function of $s/s_{\max}$. In examining the Nu profiles for pure conduction in the rhombic annulus (not shown), it is seen that for $\varepsilon = 0$, the profiles are symmetrical with the peaks in Nu occurring at $s/s_{\max} = 0$ and 1 along the hot wall and at $s/s_{\max} = 0.3$ and 0.7 along the cold wall. For positive ε the Nu

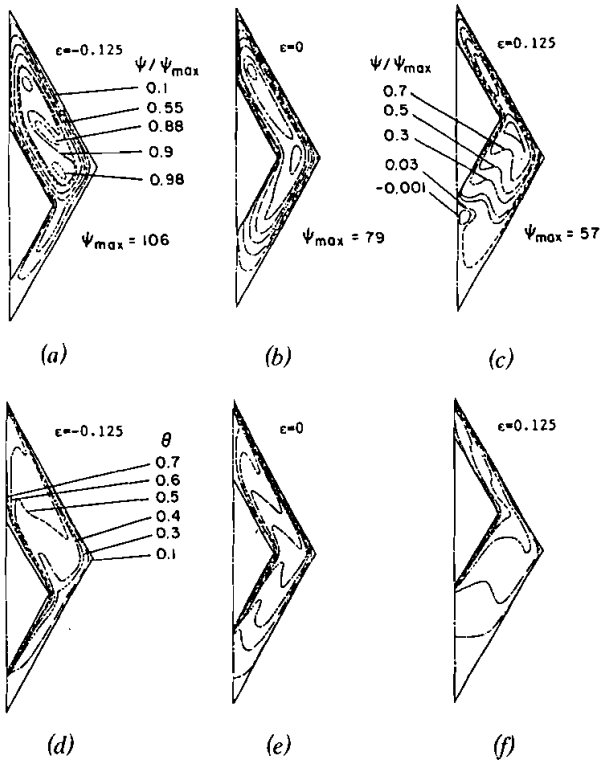

Figure 7. Streamline and isotherm plots ($E_g = 0.5$, Ra = 10^8).

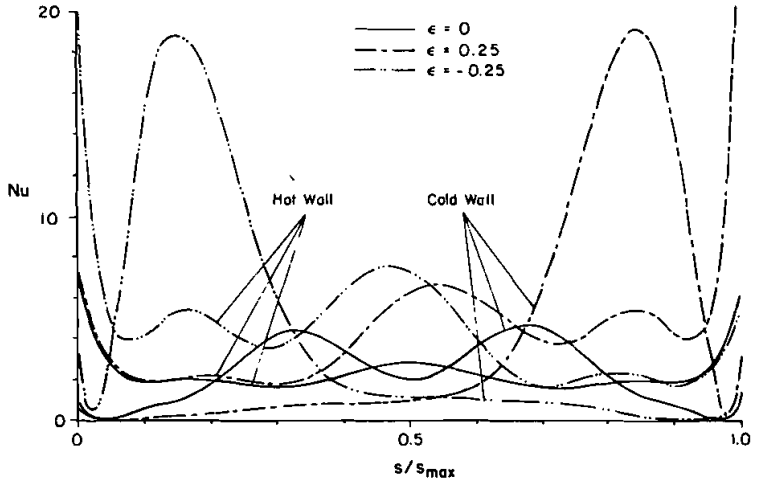

Figure 8. Local Nusselt number distribution along the hot and cold walls ($E_g = 0.75$, Ra = 10^4).

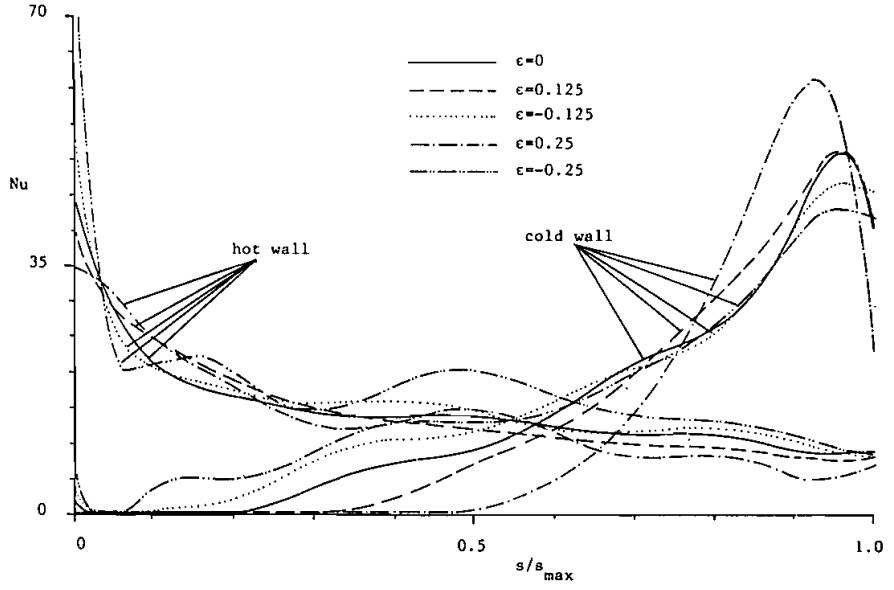

Figure 9. Local Nusselt number distribution along the hot and cold walls ($E_g = 0.75$, $Ra = 10^8$).

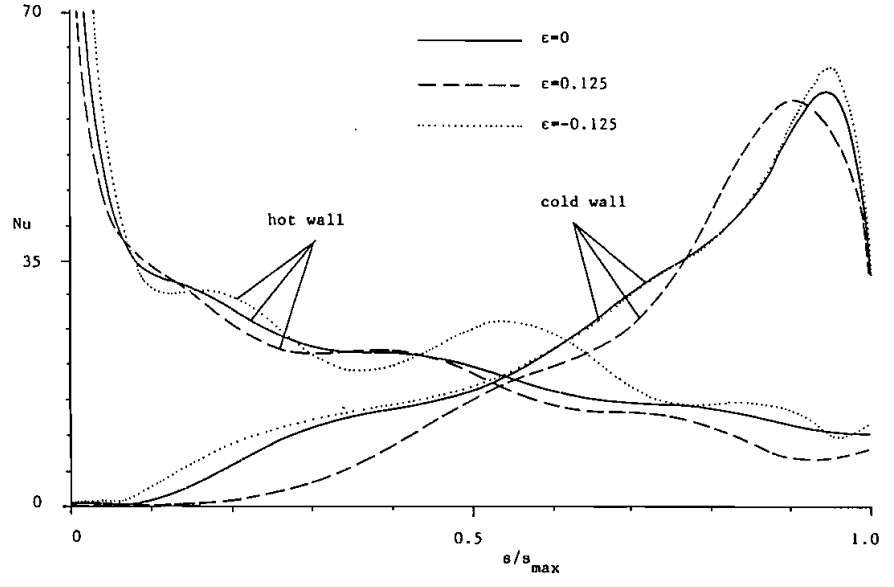

Figure 10. Local Nusselt number distribution along the hot and cold walls ($E_g = 0.5$, $Ra = 10^8$).

peak along the hot wall occurs at $s/s_{max} = 1$ and along the cold wall shifts toward $s/s_{max} = 1$. For negative ε the behavior is identically reversed, with the Nu peaks shifting toward $s/s_{max} = 0$.

At Ra = 10^4 (Figure 8) the Nu profiles are nearly identical to the profiles for the pure conduction case. At this Ra the flow pattern at all values of ε is weak, and conduction is the dominant heat transfer mode. The isotherm patterns in Figure 2 confirm this observed behavior. At high Ra (Figures 9 and 10) the Nu profiles expectedly take on a different shape. Note that the Nu values represent the effect of both two-dimensional conduction and convection. Along the cold wall, for all ε, the peak moves closer to $s/s_{max} = 1$ as Ra increases. This is expected in view of the increasing importance, at higher Ra, of the convective flow rising up along the heated rhombus and impinging on the cooled wall near $s/s_{max} = 1$. Note, as mentioned earlier, for the cylindrical annulus, a separate eddy is formed above the inner cylinder at Ra $\cong 10^5$ that shifts the Nu peak away from $s/s_{max} = 1$ [9]. For $\varepsilon = 0$, due to thermal stratification, the region $0 \leq s/s_{max} \leq 0.2$ is nearly isothermal (see Figure 4h) and is associated with very low Nu (Figure 9). As ε is increased to a positive value ($\varepsilon = 0.125$ and 0.25), an increasingly larger portion of the lower part becomes stratified and therefore leads to a larger region of s/s_{max} that is associated with very low Nu values. At the same time, since the heated inner rhombus is closer to the upper cooled surface, the cold wall Nu increase near $s/s_{max} = 1$. As ε is decreased from zero to a negative value, stratification effects in the lower portion decrease, and further, the heated inner rhombus is closer to the lower cold wall; both these effects lead to higher Nu in the lower part as ε is decreased from zero. Along the upper part of the cold wall, and in the near vicinity of the Nu peak ($s/s_{max} > 0.9$), there is a small decrease in the peak value associated with a decrease in ε from zero. As ε becomes increasingly negative, there are two counteracting effects: an increase in the strength of the flow and a reduction in the conduction heat flux to the upper cold wall as the inner rhombus is moved downward. The decrease in peak relative to the $\varepsilon = 0$ value is due to the latter effect. At $E_g = 0.5$ (Figure 10), a similar behavior is noted, except the peak Nu value does not decrease with negative ε as observed for $E_g = 0.75$. This is because as ε decreases from 0 to -0.125, the convective flow strength increases, and the associated increase in heat transfer is greater than the reduction in conduction heat transfer due to the inner rhombus moving downward.

Along the hot wall (Figures 9 and 10), the peak Nu always occurs at $s/s_{max} = 0$, where the cooled fluid from the cold wall first meets the heated surface. For cylindrical annuli, for Ra $> 5 \times 10^4$, Projahn et al. [9] report a peak near s/s_{max} of 0.5 ($\theta = 90°$). Negative ε leads to higher heat transfer peaks, since thermal stratification is reduced (leading to a stronger convective flow) and the inner rhombus is closer to the lower cooled surface (leading to a higher value of the two-dimensional conduction heat flux). In view of the stronger flow at negative ε, the Nu over most of the heated rhombus is higher than the corresponding values for the concentric case. For positive ε, due to greater stratification effects in the lower portion, the Nu peak is always smaller than the concentric value. In general, Nu values are progressively smaller for increasingly larger positive values of ε. However, due to counteracting effects (increasing ε leads to decreasing convective heat transfer and increasing conduction heat transfer from the upper portion of

the rhombus), the Nu profiles show deviations from the above-described trends for certain values of s/s_{max}.

At constant ε, Table 2 shows that $\overline{Nu}$ values increase with increasing Ra due to the increase in convection heat transfer, and with decreasing E_g value because of the increased conduction contribution to the total heat transfer. For negative ε the $\overline{Nu}$ is always greater than its corresponding value in the concentric case, and is due to the increase in conduction heat transfer in the lower part of the annulus and in the convection heat transfer in the upper part of the annulus. This increase in heat transfer over the concentric case value is higher at lower Ra (94.17% for $Ra = 10^4$ and $\varepsilon = -0.25$ compared with 11.15% for $Ra = 10^8$ and $\varepsilon = -0.25$) where conduction is the dominant mode of heat transfer. At higher values of Ra, convection heat transfer from the upper half is the primary contributor to the total heat transfer (Table 3), and this value, due to counteracting effects of increasing convection and decreasing conduction with increasingly negative ε, is less sensitive to changes in ε. Further, in light of the increase in the contribution from conduction heat transfer to the total heat transfer, this increase in heat transfer with a decrease in ε from 0 is generally greater at smaller E_g values.

For positive ε the picture is somewhat different. At low Ra, positive ε results in an increase in the overall heat transfer. This occurs due to the dominance of the conduction heat transfer mode at low values of Ra, and conduction heat transfer on the upper side increases as the rhombic enclosures approach each other. As Ra is increased, the increase in conduction as ε increases from zero is countered by the decrease in convection heat transfer due to greater thermal stratification effects. At a certain critical value of Ra (between 10^5 and 10^6 for $\varepsilon = 0.125$ and $E_g = 0.75$, for example), the increase in conduction heat transfer due to an increase in ε will be equal to the associated decrease in convection heat transfer. This critical value of Ra depends on E_g and ε. Beyond this critical value, the increase in conduction cannot offset the decrease in convection created by the large stagnant area in the lower part of the annulus, and the net effect of positive ε is a decrease in $\overline{Nu}$.

Table 3 shows the contribution of the lower and upper parts of the cold wall to the total heat transfer for $E_g = 0.75$. For negative eccentricity the general trend is similar to that obtained in the concentric case, where the contribution of the upper part to the total heat transfer is higher when convection is important and is lower when conduction is important. The contribution of the lower part is seen to increase with increasingly negative ε due to the decrease in the distance between the two rhombic enclosures, which promotes conduction heat transfer, and because convection, which is important over the upper part of the lower wall, becomes stronger at larger negative values of ε. For positive ε, however, the highest contribution is always to the upper half due to higher conduction (walls are closer in the upper half). Due to thermal stratification in the lower half, the heat transfer contribution to the lower half decreases with increasing ε. Nu variations over the lower and upper parts of the hot wall show similar behavior and are not presented.

In the Ra regime where convection effects are clearly important ($Ra \geq 10^6$), the following correlations are applicable with less than 15% error:

$$Nu = 0.125\,(Ra)^{0.24}\,(E_g)^{-1.1} \qquad \varepsilon = 0 \qquad (15a)$$

$$\mathrm{Nu} = 0.125\,(\mathrm{Ra})^{0.24}\,(E_g)^{-1.1}\,e^{(\varepsilon^2-\varepsilon/2)} \qquad \varepsilon < 0 \qquad (15b)$$

$$\mathrm{Nu} = 0.125\,(\mathrm{Ra})^{0.24}\,(E_g)^{-1.1}\,e^{(2\varepsilon^2-0.85\varepsilon)} \qquad \varepsilon > 0 \qquad (15c)$$

CONCLUDING REMARKS

A numerical study is made to determine the influence of eccentricity on the heat transfer and flow in an eccentric rhombic annulus. The following major conclusions can be drawn from this study.

1. At low Ra ($< 10^5$ in this study), where thermal stratification is not important, negative or positive ε leads to an increase in the flow strength in the region (upper or lower) with the greater flow cross-sectional area. With increasing ε, there is an associated increase in the overall heat transfer.
2. At higher Ra, flow-induced thermal stratification effects in the lower half of the annulus are promoted. With positive ε, thermal stratification in the lower half increases, leading to flow retardation and reduction in heat transfer. The opposite effect occurs at negative ε and leads to a stronger convective flow and greater heat transfer.
3. For positive ε there is a critical Ra beyond which the overall convection heat transfer progressively decreases with increasing ε. For the range of parameters in this study, it was observed that this critical Ra increases with decreasing E_g values. Convection heat transfer increases with increasingly negative values of ε at all Ra.
4. At lower Ra the Nu distribution is conductionlike, with the Nu peak along both walls shifting upward with positive ε and downward with negative ε. At higher Ra the peak along the hot wall occurs at $s/s_{\max} = 0$ and that along the cold wall near $s/s_{\max} = 1$ for all values of ε.
5. At lower Ra ($\mathrm{Ra} < 10^5$ for $\varepsilon = -0.125$ and $\mathrm{Ra} < 10^6$ for $\varepsilon = -0.25$), and for negative ε, the heat transfer contributions from the lower half are greater than those from the upper half; the reverse is true for $\varepsilon > 0$. At higher Ra, where convection heat transfer is important, the heat transfer contribution from the upper half is always greater.

REFERENCES

1. S. Ostrach, Natural Convection in Enclosures, *ASME J. Heat Transfer*, vol. 110, pp. 1175–1190, 1988.
2. T. H. Kuehn and R. J. Goldstein, An Experimental and Theoretical Study of Natural Convection in the Annulus between Horizontal Concentric Cylinders, *J. Fluid Mech.*, vol. 74, p. 695–719, 1976.
3. T. H. Kuehn and R. J. Goldstein, Numerical Solution to the Navier-Stokes Equations for Laminar Natural Convection about a Horizontal Isothermal Circular Cylinder, *Int. J. Heat Mass Transfer*, vol. 23, pp. 971–979, 1980.
4. J. R. Custer and E. J. Shaughnessy, Thermoconvective Motion of Low Prandtl Number Fluids within a Horizontal Cylindrical Annulus, *ASME J. Heat Transfer*, vol. 99, pp. 596–602, 1977.

5. B. Farouk and S. I. Guceri, Laminar and Turbulent Natural Convection in the Annulus between Horizontal Concentric Cylinders, *ASME J. Heat Transfer*, vol. 104, pp. 631–636, 1982.
6. A. Castrejon and D. B. Spalding, An Experimental and Theoretical Study of Transient Free-Convection Flow between Horizontal Concentric Cylinders, *Int. J. Heat Mass Transfer*, vol. 31, pp. 273–284, 1988.
7. R. Kumar, Study of Natural Convection in Horizontal Annuli, *Int. J. Heat Mass Transfer*, vol. 31, pp. 1137–1148, 1988.
8. P. M. Kolesnikov and V. I. Bubnovich, Non-Stationary Conjugate Free-Convective Heat Transfer in Horizontal Cylindrical Coaxial Channels, *Int. J. Heat Mass Transfer*, vol. 31, pp. 1149–1156, 1988.
9. U. Projahn, H. Reiger, and H. Beer, Numerical Analysis of Laminar Natural Convection between Concentric and Eccentric Cylinders, *Numer. Heat Transfer*, vol. 4, pp. 131–146, 1981.
10. C. H. Cho, K. S. Chang, and K. H. Park, Numerical Simulation of Natural Convection in Concentric and Eccentric Horizontal Cylindrical Annuli, *ASME J. Heat Transfer*, vol. 104, pp. 524–530, 1982.
11. J. Prusa and L. S. Yao, Natural Convection Heat Transfer between Eccentric Horizontal Cylinders, *ASME J. Heat Transfer*, vol. 105, pp. 108–116, 1983.
12. E. K. Glakpe, C. B. Watkins, and J. N. Cannon, Constant Heat Flux Solutions for Natural Convection between Concentric and Eccentric Cylinders, *Numer. Heat Transfer*, vol. 10, pp. 279–295, 1980.
13. C. J. Ho and Y. H. Lin, Natural Convection Heat Transfer of Cold Water within an Eccentric Horizontal Cylindrical Annulus, *ASME J. Heat Transfer*, vol. 110, pp. 894–900, 1988.
14. D. Naylor, H. M. Badr, and J. D. Tarasuk, Experimental and Numerical Study of Natural Convection between Two Eccentric Tubes, *Int. J. Heat Mass Transfer*, vol. 32, pp. 171–181, 1989.
15. K. S. Chang, Y. H. Won, and C. H. Cho, Patterns of Natural Convection around a Square Cylinder Placed Concentrically in a Horizontal Cylinder, *ASME J. Heat Transfer*, vol. 105, pp. 273–280, 1983.
16. J. H. Lee and T. S. Lee, Natural Convection in the Annuli between Horizontal Confocal Elliptic Cylinders, *Int. J. Heat Mass Transfer*, vol. 24, no. 10, pp. 1739–1742, 1981.
17. R. O. Warrington and R. E. Powe, Natural Convection between Bodies and Their Enclosure, *Int. J. Heat Mass Transfer*, vol. 28, no. 2, pp. 319–330, 1985.
18. R. D. Boyd, Steady Natural Convection Heat Transfer Experiments in a Horizontal Annulus for the United States Spent Fuel Shipping Cask Technology Program, Sandia National Laboratory Report, SAND-80-1057, 1981.
19. E. K. Glakpe and A. Asfaw, Prediction of Two-Dimensional Natural Convection in Enclosures with Inner Bodies of Arbitrary Shapes, *Numer. Heat Transfer*, vol. 20, no. 3, pp. 279–296, 1991.
20. F. Moukalled, H. Diab, and S. Acharya, Numerical Simulation of Laminar Natural Convection in Concentric Ducts of Rhombic Cross Sections, *Numer. Heat Transfer*, vol. 24, pp. 89–108, 1993.
21. J. F. Thompson, *Numerical Grid Generation*, North-Holland, Amsterdam, 1982.
22. S. V. Patankar, *Numerical Heat Transfer and Fluid Flow*, Hemisphere, New York, 1980.
23. C. M. Rhie and W. L. Chow, Numerical Study of the Turbulent Flow Past an Airfoil with Trailing Edge Separation, *AIAA J.*, vol. 21, pp. 1525–1532, 1983.